Applied Physics B (2020) 126:96
https://doi.org/10.1007/s00340-020-07449-w

Applied Physics B
Lasers and Optics

Theoretical and experimental study of a surface plasmon sensor based on Ag-MgF_2 grating coupler

Saeid Nazem[1] · Mohammad Malekmohammad[1] · Mahmood Soltanolkotabi[1]

Received: 5 October 2019 / Accepted: 24 April 2020 / Published online: 2 May 2020

Abstract
To achieve a high-sensitivity surface plasmon resonance sensor, a sensor based on Ag-MgF_2 grating was designed and fabricated. A suitable-thickness MgF_2 was suggested to prevent the oxidation of silver while avoiding reducing its plasmonic properties. The combination of an interference lithography approach, the material used for the fabrication of grating, and angular interrogation method led to a less costly sensor. The sensitivity and figure of merit of the proposed sensor approached 85.61 deg/RIU and 51 RIU^{-1}, respectively, which is higher than the experimental values reported so far for grating-based sensors. It was shown that by optimization of the silver-based structure, it has great potential for use in sensor applications. It was observed that based on the made grating pattern, the numerical results were closer to experimental results by considering the grating pattern in a sine form. The effect of temperature on sensor performance was experimentally investigated. It was demonstrated that the change in the resonance angle with the temperature in this structure was equal to 0.02 deg/°C and it was also experimentally shown that temperature changes in the analyte refractive index had the most effect on the variations of the SPR response with temperature.

1 Introduction

Surface plasmon polaritons (SPP) are electromagnetic (EM) waves propagating at the interface of a metal and a dielectric material. When a conductor's electron plasma oscillations are coupled with EM fields, a strong absorption of EM waves occurs. By changing the refractive index (RI) of the surrounding environment of the metallic film, the propagation constant of the surface plasmon will change. This change can appear by the shift in the peak position of surface plasmon resonance (SPR). SPR sensor technology has attracted a lot of attention not only due to its high sensitivity, but also because of its label-free, real-time, and fast detection as well as its reduction of electromagnetic interference [1, 2].

Many applications of surface plasmon sensors have been reported in various fields of chemistry [3], gas analysis [4], biology [5], medical diagnostics [6], environmental monitoring [7], and food safety [8–10]. These wide-ranging applications have led researchers to increase the sensitivity of these sensors by various methods.

✉ Mohammad Malekmohammad
m.malekmohammad@sci.ui.ac.ir

[1] Department of Physics, Faculty of Science, University of Isfahan, Hezar Jerib Street, Isfahan, Iran

The incident light on a metal–dielectric interface could not typically excite SPs. Therefore, exciting SPs needs to be done artificially. It can be done by a prism [11] or grating coupling [12, 13]. As an instance, in reference [11], using a graphene SiO_2/Si structure and prism coupling method, a high resolution plasmonic sensor for the thickness of 0.335 nm of graphene and incident angle of 62.5° was obtained.

Surface plasmons coupled on metallic gratings are also used to improve the performance of various optoelectronic devices such as detectors [14], lasers [15], and solar cells [16]. However, it has been reported that the major applications of these devices are in optical sensors. Therefore, there has recently been a lot of research to improve the sensitivity of grating sensors so that they can replace prism-based sensors.

The first high-sensitivity surface plasmon sensor was introduced in 1999 by Homola and colleagues without the use of molecular labels [17]. Subsequently, surface plasmon sensors are widely used in the analysis of bimolecular interactions and the detection of chemical and biological analytes. On the other hand; a living cell is a complex structure, which contains numerous organelles with different refractive index. For example, the refractive index of cytoplasm is normally 1.35–1.38, and the index of nucleus is around 1.39.

However, the protein concentration within the cell components mainly determines the effective refractive index of cells because of the large amount and high refractive index of 1.50–1.58 [18, 19].

With the advent of new technologies, an interest has emerged toward making sensors which are capable of detecting specific sensor responses from uncertain responses such as temperature fluctuations, analyte combinations, and so on. In 2005, the combination of a prism and a dielectric grating was proposed to improve the efficiency of surface plasmon wave transmission (which increased to 68%) [20]. In reference [21], nanograting surface plasmon resonance (NGSPR) sensors have been proposed. In 2008, surface plasmon sensors based on palladium-coated metal grating were used to detect hydrogen gas [22]. In 2010, Kan et al. presented the construction of an integrated sensor by Au grating on a Si prism for point-of-care applications [23]. In this structure, the negative orders of the diffracted waves of grating were used. In 2011 [24], another type of sensor was introduced including nanogratings with very narrow grooves (less than 15 nm). In 2012, using interference lithography (IL) based on pulsed laser, a large area submicron grating on Au was constructed by Arriola et al. to be used as a sensor [25].

In reference [26], to improve the performance of an Au grating surface plasmon sensor, instead of a perpendicular incident light, an oblique incident light was applied. In this reference, the sucrose aqueous solutions at the concentrations of 0, 5, 10, 15, 20, 25, 30, 40, 50, and 60 wt%, and the corresponding refractive indexes 1.3330, 1.3372, 1.3478, 1.3556, 1.3639, 1.3740, 1.3812, 1.4000, 1.4200, and 1.4419, respectively, were also investigated.

Many researchers have tried to improve the sensitivity of SPR sensors based on metal grating so that they can detect small changes in the RI of analyte. In plasmonic grating structures, using hybrid structures, Ag is optimized and preferred to Au despite its chemical instability because of its high scattering efficiency and narrow bandwidth. In fact, Au is more stable and more sensitive than Ag. However, the full width at half maximum (FWHM) of its SPR spectrum is large. Therefore, in most sensing applications, Au is less accurate than Ag. Hence, many efforts have been made to increase the stability of Ag including hybrid metal structures. In reference [27], it has numerically been shown that angular sensitivity can reach 346 deg/RIU with a quality factor of 97.46 RIU^{-1} using a bimetallic structure consisting of a silver grating on a metal film where RIU is the refractive index unit. In addition to sensor applications, bimetallic and hybrid structures have also been used in other applications such as solar cells [28, 29]; so that, in reference [30], Ag: Zn and Ag: Mg nanocomposites were used to improve the optical and electrical properties of organic thin-film solar cells.

In this paper, a high quality SPR sensor based on silver grating is designed and fabricated. The grating pattern is implemented by interference lithography which is faster and less costly than other methods such as electron beam lithography (EBL), ion beam lithography (IBL), and nanoimprint lithography (NIL). We present MgF_2 coating to avoiding the oxidation of silver while maintaining the SPR response. The positive diffraction orders of metallic grating are used to excite the surface plasmons and the sensor parameters are examined. The angular interrogation approach studied here is less costly than the spectral interrogation mode. The results show that the proposed sensor has higher sensitivity and quality factor than the experimental cases reported so far. The effect of temperature on the operation of the sensor is also investigated.

2 Theory of a grating-based SPR sensor

When the TM-polarized light at the wavelength of λ is incident on a grating, in some directions, the surface plasmon wave begins to propagate in the metal–dielectric interface. This is due to the coupling of the incident field and the oscillation of the free electrons of metal. This coupling leads to a reflection dip in the zero-order angular spectrum. Figure 1 shows a schematic diagram of a grating coupled SPR sensor model using angular interrogation.

The radiation on grating in various angles produces a series of diffracted waves. In the angle at which the diffracted wave vector is parallel to the surface plasmon wave vector, the SPR excitation occurs [17]:

$$\mathrm{k}_0 n_a \mathrm{Sin}\theta_{res} + m\frac{2\pi}{\Lambda} = \pm \mathrm{k}_0 \sqrt{\frac{n_a^2 \varepsilon_m}{n_a^2 + \varepsilon_m}} \tag{1}$$

where m is an integer, θ_{res} is the resonance angle, k_0 is the free space wave vector of optical wave, n_{a} is the RI of the analyte, ε_{m} is the permeability of metal, and Λ is the period of the grating. The + and − signs correspond to the diffracted modes with the order of $m > 0$ and $m < 0$, respectively. Since the effective surface plasmon excitation requires that $\varepsilon_m >> n_a^2$, the limitation on the grating period can be expressed as follows [22]:

$$\left\{ \begin{array}{ll} \Lambda > \dfrac{\mathrm{m}\lambda}{n_a} & m > 0 \\ \dfrac{|\mathrm{m}|\lambda}{2n_a} < \Lambda < \dfrac{|\mathrm{m}|\lambda}{n_a} & m < 0 \end{array} \right\} \tag{2}$$

Periodic grating sensors provide a distinct change either in the intensity of diffracted light or in the frequency of optical resonance in response to variations in the RI of the surrounding environment. The principal mechanism of this optical signature is the well-known phenomenon called 'Bragg scattering'. Although this process provides useful

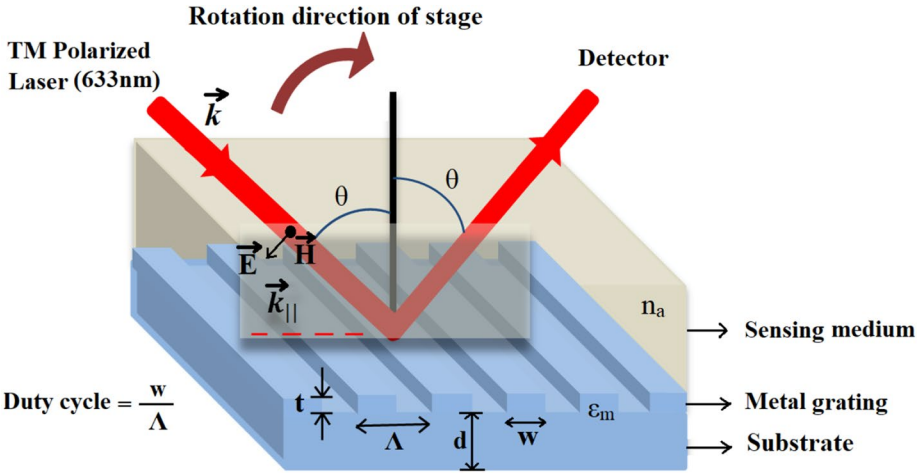

Fig. 1 Schematic diagram of a grating coupled SPR sensor in angular modulation mode

frequency-selective responses for colorimetric detection, the ability of light waves to interact with absorbed or chemically bound analytes present on the surface of these sensors is intrinsically limited. In fact, Bragg scattering is a first-order process in surface scattering perturbation theory [31] and the scattered photons easily escape from a periodic surface within well-defined spectral bands and without prolonged interaction with the sensing layer. Therefore, a surface plasmon resonance sensor can yield a label-free detection of various molecular analytes and protein dynamics. Label-free sensor is usually based on physical parameter detection such as optical, electrical, and acoustic. The surface plasmon resonance sensor designed in this work is a label-free detection method which could detect the molecular binding and dissociation without any label on samples.

Angular sensitivity, S and figure of merit (FOM_θ) are important parameters in the evaluation of sensor performance. Angular sensitivity is defined as the ratio of the shift of resonance angle $\Delta\theta_{res}$ to the change in the RI of the analyte Δn_a:

$$S = \frac{\Delta\theta_{res}(\text{deg})}{\Delta n_a(\text{RIU})} \tag{3}$$

where RIU is the refractive index unit. FOM_θ is defined as the ratio of sensitivity to resonant width:

$$FOM_\theta = \frac{S\left(\frac{\text{deg}}{\text{RIU}}\right)}{\text{FWHM(deg)}} \tag{4}$$

In a broad FWHM, it is difficult to distinguish among small variations in the amount of dip.

Using the two-dimensional finite-difference time-domain (2D-FDTD) method for solving Maxwell's equations, the angular SPR treatment of the grating-based sensor was calculated. The computational domain consists of a single period of the grating. The mesh size in this simulation was taken 5 nm in two dimensions which meets the necessary resolution of FDTD simulation. We used the periodic boundary condition along the periodic direction and the perfect matched layer (PML) absorption boundary condition at the top and bottom boundaries. Throughout the article, we only give attention to the plane wave with TM polarization. Silver permeability was considered as ε_m (633 nm) = − 18.23 + 0.482*i* [32]. Figures 2 and 3 show the simulated SPRcurve of a grating-based sensor for the periods, Λ, of 900, 1200, and 1600 nm with a silver thickness of 65 nm in a rectangular and sinusoidal pattern, respectively. The source of excitation was the TM-polarized light at a wavelength of 633 nm. As can be seen, the dip strength is longer for sinusoidal pattern than rectangular pattern. Also, Fig. 3 shows that as periodicity increases, the resonance

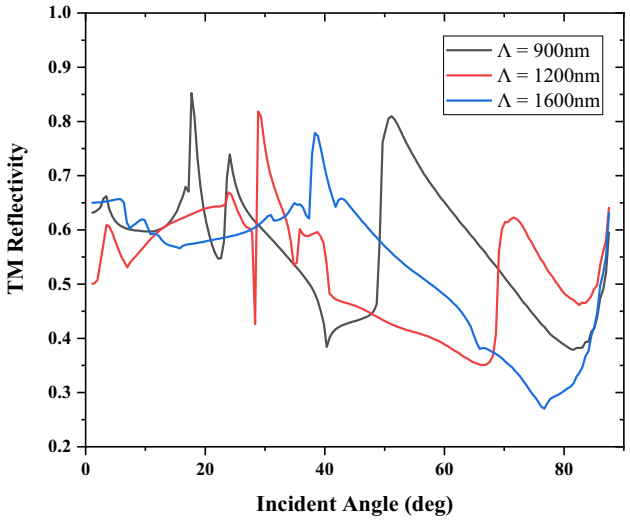

Fig. 2 Simulated SPR response for different periods, Λ, of plasmonic grating (900, 1200 and 1600 nm) with a silver thickness of 65 nm in a rectangular pattern. The data are for glass substrates, duty cycle 50% and air analyte

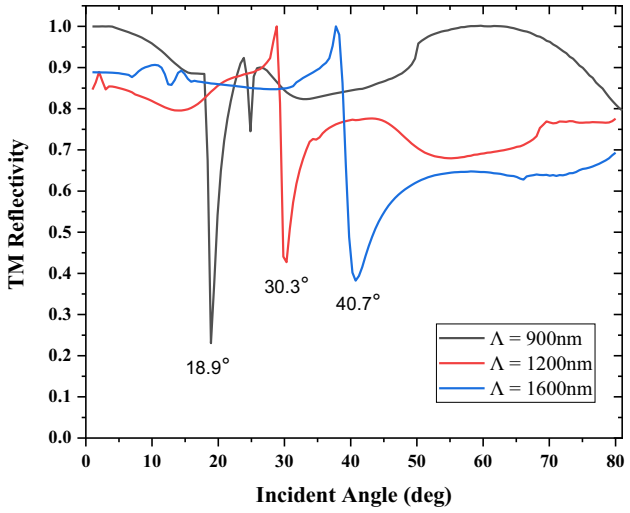

Fig. 3 Simulated SPR response for different periods, Λ, of plasmonic grating (900, 1200 and 1600 nm) with a silver thickness of 65 nm in a sinusoidal pattern. The data are for glass substrates and air analyte

angle shifts to larger values. This limits the dynamic range of the sensor in measuring the large values of RI. On the other hand, as the period increases, the resonance FWHM also increases. It is worth noting that for keeping the other parameters constant, the SPR response for different periods depends on the thickness of the metal grating. The SPR curve for the grating with a period, Λ, of 900 nm versus the different thicknesses of silver taking account to a sinusoidal pattern for Ag grating has been shown in Fig. 4. As can be seen in the figure, the optimum thickness of the silver grating

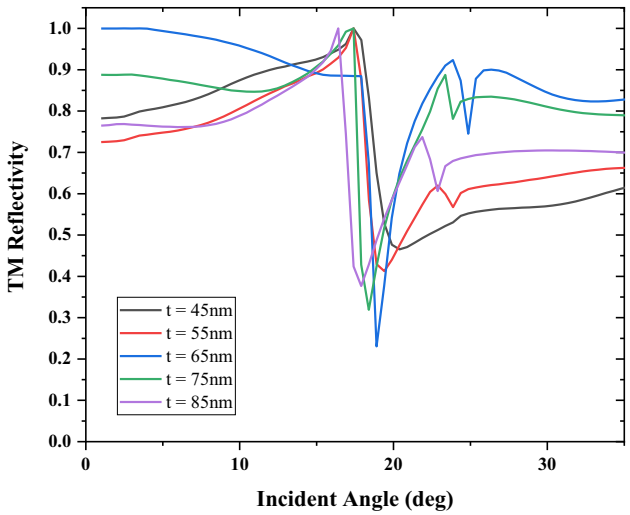

Fig. 4 The simulated SPR response of a plasmonic grating with a period, Λ, of 900 nm for different thicknesses of silver (45, 55, 65, 75 and 85 nm) with taking account to a sinusoidal pattern for Ag grating. The data are for glass substrates and air analyte

is 65 nm. Because for this thickness, the resonance width was also narrower in addition to the larger dip strength. On the other hand, with an increase in the thickness of silver, the angle of excitation decreases slowly. Therefore, among the structures studied, the optimum case, a grating sensor with a period, Λ, of 900 nm and an Ag grating thickness of 65 nm was considered as input data for the experimental mode with the excitation wavelength of 633 nm. In the next section, we will see that the results of the sensor simulation with the grating sinusoidal pattern are in better agreement with the experimental results and the method of fabrication selected.

3 Experimental details and results

3.1 Device fabrication

To fabricate the chip, a 500-nm thick AZ1505 photoresist (MICROCHEMICALS) was coated on a borosilicate glass substrate by a spin coater at 4000 rpm after cleaning the substrate. Then it was soft baked for 90 s on a hotplate at 110 °C to remove the remaining solvent in the photoresist. The sample was then exposed by the interference lithography setup shown in Fig. 5. In this configuration, the light beam from a continuous-wave and single-longitudinal mode solid state laser with a wavelength of 360 nm (MSL-FN-360, CNILASER) is split into two parts by a beam splitter (BS) after passing a polarizer (P). These beams reach the substrate after passing through a spatial filter (consisting of a lens (L) with a focal length of 50 mm and a pinhole (D) with a diameter of

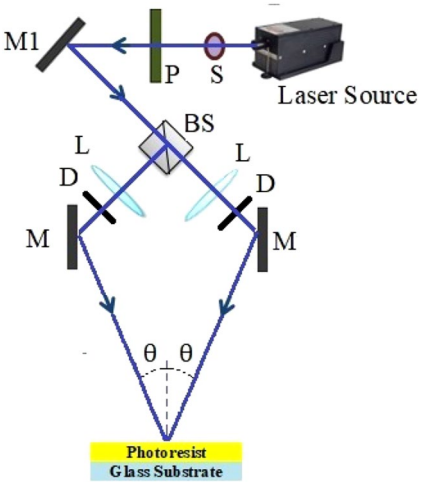

Fig. 5 Interference lithography setup: The light beam from a continuous-wave and single-longitudinal-mode solid state laser with a wavelength of 360 nm is split into two parts by a beam splitter (BS) after passing a polarizer (P). These beams reach the substrate after passing through a spatial filter [consisting of a lens (L) and a pinhole (D)] and a mirror (M) so that both beams make an angle θ with the normal line on the substrate. Exposure time can be controlled using the shutter(S)

10 µm) and a mirror (M) so that both beams make an angle θ with the normal line on the substrate. The period of the structure was obtained from the relation $\lambda/2\sin\theta$ in which λ is the wavelength of the laser beam. Using the shutter (S), the exposure time was controlled. The samples were exposed to this method at periods, Λ, of 900, 1200, and 1600 nm and with exposure times of 17, 20, and 25 s, respectively. Then the sample was post-exposure baked for 60 s at 110 °C on a hotplate and was then immersed in an AZ351B developer (MICROCHEMICALS) with a ratio of 1:5 (AZ351B:H2O) for 60 s. Finally, after being washed with de-ionized water, it was dried with nitrogen. Subsequently, by the thermal evaporation method, 5 nm of chromium, 65 nm of silver, and 15 nm of MgF_2 were deposited, respectively, on the samples at a rate of 1 Å/s. Since the sensitivity of the sensor decreases due to oxidation, to prevent silver oxidation, MgF_2 is coated on the silver grating. Chromium was used for better adhesion of silver to the substrate. At the end, the samples were lifted off by acetone to remove the remainder of the photoresist. Figure 6 shows the fabrication steps in the process.

The morphology of the samples was determined by an atomic force microscope (AFM). AFM topography image and cross-sectional analysis of Ag-MgF_2 gratings with different periods have been shown in Fig. 7a–c. As you can see in the Fig. 7a–c, the metal gratings made by interference lithography based on continuous-wave laser, wet-etching, and then lift-off are sinusoidal in shape. The exact values of the periods of the constructed gratings were measured by AFM and were 895, 1190, and 1610 nm.

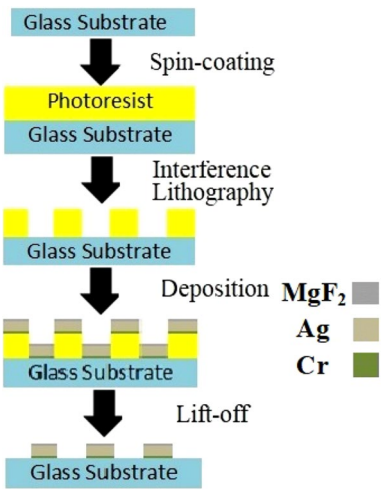

Fig. 6 Fabrication steps of SPR sensor chip: A glass substrate is cleaned by 2-propanol and pure acetone. The AZ1505 photoresist is spin-coated on the substrate and pre-baked. Then, the sample is exposed using an interference lithography setup, post-exposure baked, and developed. Chromium, silver and MgF_2 layers are deposited on the sample, respectively. Finally, the sample is lifted off by acetone

Also, an electron microscope image was obtained to obtain the confidence of the sinusoidal structure of the grating. A side view of micro objects produced by a FESEM has been shown in Fig. 8. This confirms that the grating made by interference lithography method based on a continuous-wave laser, the subsequent use of a wet etching method (that is isotropically etching) and lift-off, has created a sinusoidal structure.

3.2 SPR measurement

The sensor chip was inserted into a chamber. This chamber includes a mounting for chip installation, an optical window for passing light beams, and two valves for the inlet and outlet of various analytes. The SPR sensor was placed on a rotational stage and controlled the angle of the incident light on the sensor with a precision of 0.25°. Figure 9 illustrates the layout of the SPR measurement. The light of a Helium–Neon laser 633 nm (SUPA13L, SUNSHID) was TM-polarized by a polarizer and was incident through the optical window to the chip surface. The zero order reflectivity of the sensor chip was measured by a photo detector (S120VC, THORLABS). All the measurements were carried out at a temperature of 23 °C and the ambient humidity was within the range of 11–15%. When the remaining electrical and software components of the system are taken into account, the response time of the sensor depends on the angular scan rate and the angular range studied. By knowing the approximate refractive index of the analyte, the angular range under investigation can be reduced, thus reducing the response time of the sensor. In this study, the sensor response time was approximately 120 s due to the angular scan speed of 0.5°/s and the considered angular range.

The zero-order reflectivity curve at various angles is shown in Fig. 10 for gratings with the periods, Λ, of 895, 1190, and 1610 nm. As is seen in the figure, dip strength decreases with increasing period. Also, with increasing period, the resonance angle shifts towards larger angles. To have a sensor with a wide dynamic range (1–1.6 RIU), the resonance needs to occur at low incident angles which are possible in a grating with a period, Λ, of 895 nm. Also, for this period, the dip strength is higher and the resonance width narrower. The above observations are in good agreement with the results of the Fig. 3. The larger incident angle at the metal-air interface, due to the increase in light diffraction with increasing incident angle, results in a decrease in the reflection intensity, thereby reducing the dip strength. Therefore, the grating with a period, Λ, of 895 nm was selected as the proposed sensor.

Sensor sensitivity to RI was determined using various analytes including water, ethanol, 2-propanol, and ethylene glycol with the corresponding refractive index of 1.332,

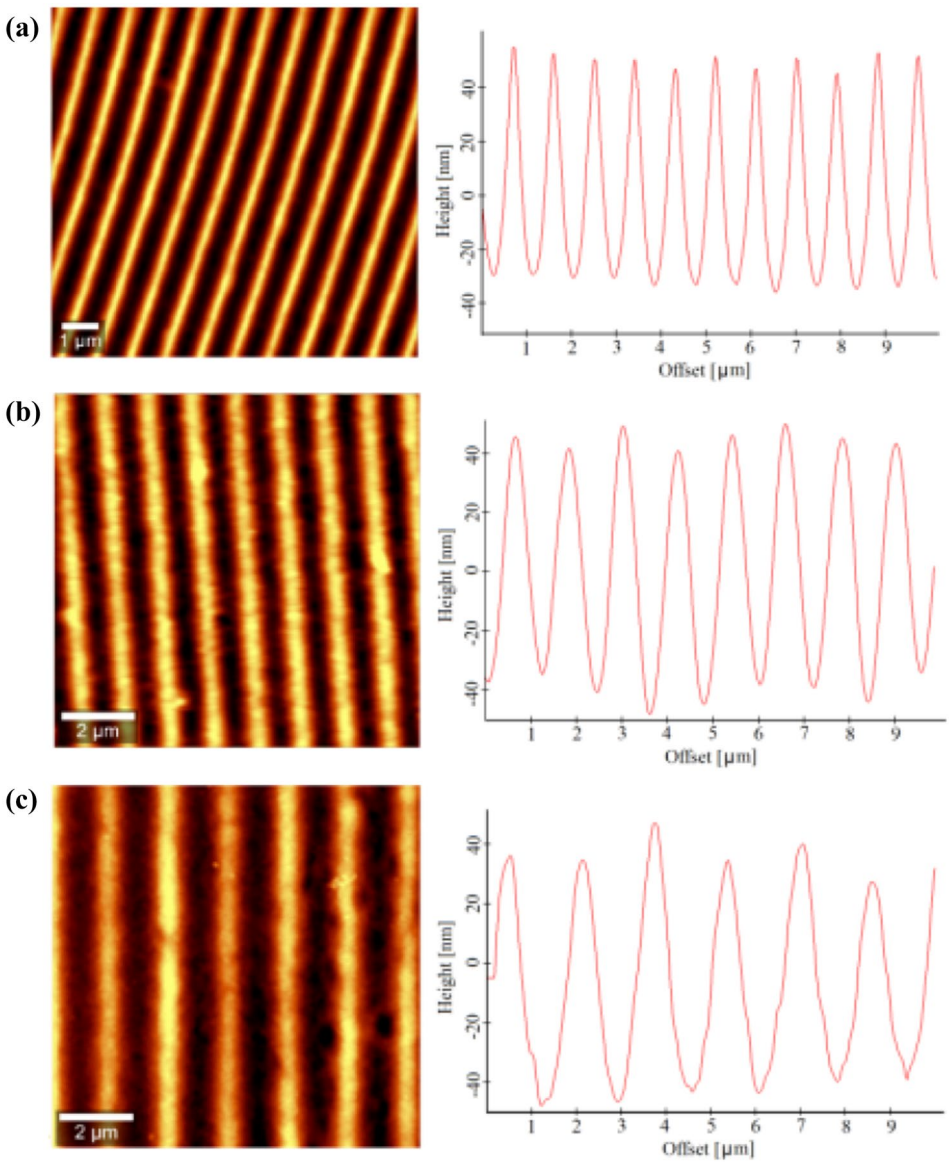

Fig.7 AFM topography image and cross-sectional analysis of Ag-MgF_2 gratings made with different periods, Λ, **a** 895 nm, **b** 1190 nm, **c** 1610 nm

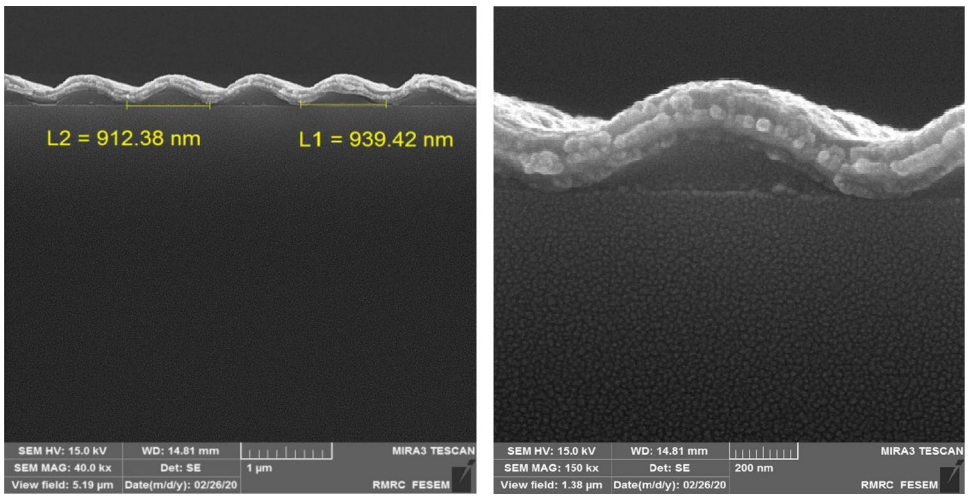

Fig. 8 Side-view FESEM images of sinusoidal surface of the fabricated MgF_2 grating for the grating with a period, Λ, of 900 nm

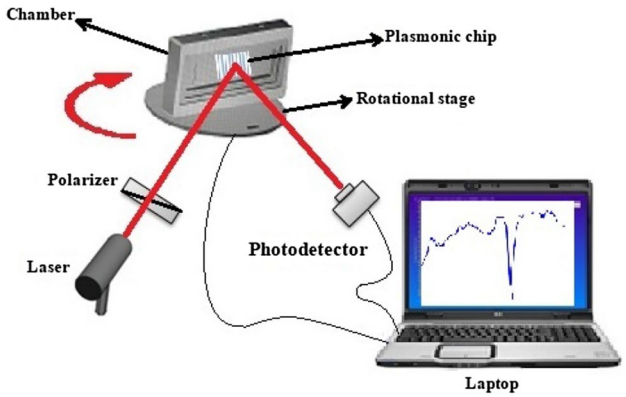

Fig. 9 Setup of SPR measurement

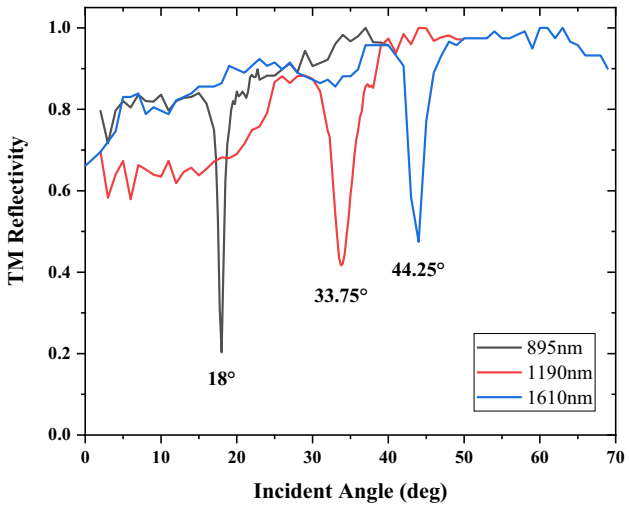

Fig. 10 Experimental reflectivity spectra for TM-polarized light at different angles of incidence for the periods, Λ, of 895, 1190, and 1610 nm

1.360, 1.376, and 1.4301 (Fig. 11). As can be seen in the figure, by increasing the analyte refractive index, the SPR angle shifts to larger angles. Also, the dip strength increases as the RI of analyte increases. The data obtained for the different analytes have been normalized to their maximum extent during each measurement.

In Table 1, the numerical values of the performance of the proposed sensor extracted from Fig. 11 are given. Based on the data in Table 1 and the Eqs. (3) and (4), the variations of the resonance angle, FWHM, and FOM with the changes of RI are shown in Fig. 12a–c. As is seen in Fig. 12a, with an increase in the RI of the analyte, θ_{res} shifts to larger angles which is in accordance with the theoretical predictions for $m > 0$ mode. As can be observed, by varying the RI of the surrounding environment from 1.332 to 1.4301, the resonance angle is shifted from 40.5° to 48.75°. The fitting line between the resonance angle and RI of the analyte indicates that the sensitivity is equal to approximately 85.6 deg/RIU with a good linearity whereas in reference [23], a sensitivity value of 28.5 deg/RIU was reported for the device with 395-nm pitch grating. Fluids with a refractive index of up to 1.6 can be detected by the proposed sensor. As can be seen in Fig. 12b, FWHM increases as the RI of analyte increases. Narrower and deeper resonance reflection dips provide the ability to determine the minimum reflection angle accurately. The FOM variations with the analyte refractive index (Fig. 12c) show that FOM decreases with increasing RI of the surrounding environment which is affected by the FWHM variations. So that with the change of n_a from 1.332 to 1.4301, the FOM decreases from 51 to 22.22 RIU^{-1}, while at reference [26], the reported FOM value was up to about 12.

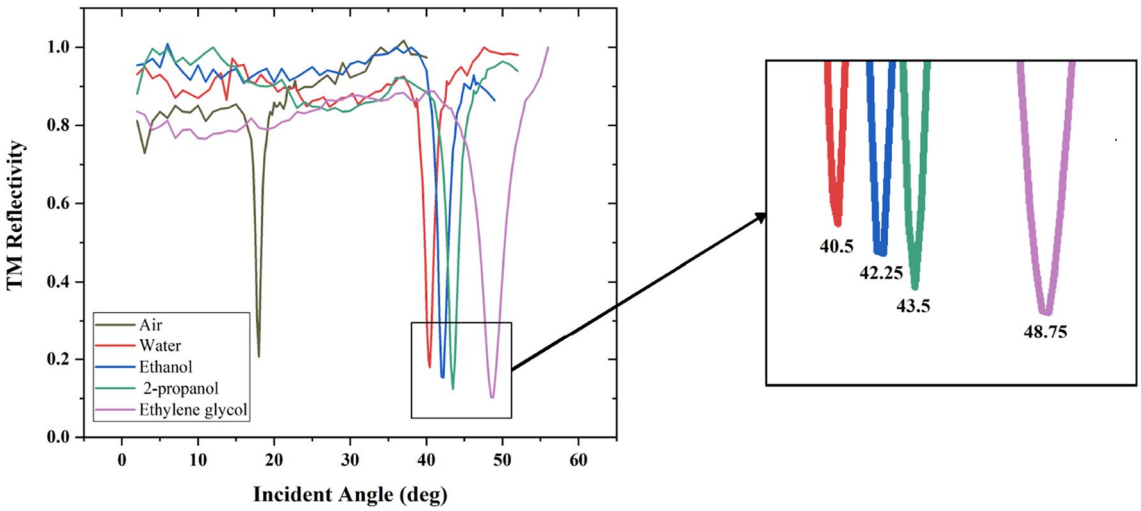

Fig. 11 Experimental SPR curves for various analytes for the Ag-MgF_2 grating with a period, Λ, of 895 nm

Table 1 The comparison of refractive index, resonance angle and FWHM of the proposed SPR sensor for different analytes

Analyte	Refractive index (RIU)	Resonance angle (°)	FWHM (°)
Air	1.0003	18.0	0.87
Water	1.332	40.5	1.33
Ethanol	1.360	42.25	1.53
2-propanol	1.376	43.5	1.6
Ethylene glycol	1.4301	48.75	3.22

3.3 Temperature effect

The ambient temperature fluctuations during the operation of the sensor can have a significant effect on the performance of the SPR sensor. Actually, due to the scattering of photon-electron and electron–electron, as well as thermo-optical effects and thermal expansion, metal and dielectric properties will change. One of the advantages of a grating-based SPR sensor over a prism-based sensor is its lower sensitivity to the components of the system. As an instance, changes in the RI of the prism with temperature in a prism-based SPR sensor can have a significant effect on the performance of the sensor. In 2019, Lou et al. measured the changes in RI and temperature simultaneously for angular analysis mode using sensitivity matrix formation in a prism-based sensor [33]. In reference [34], the effect of temperature changes on the resolution of prism-based and grating-based SPR sensors in both angular modulation and wavelength modulation has been theoretically investigated.

In the current study, the temperature changes of the SPR response of proposed sensor were experimentally considered using an air cooling system equipped with a combination

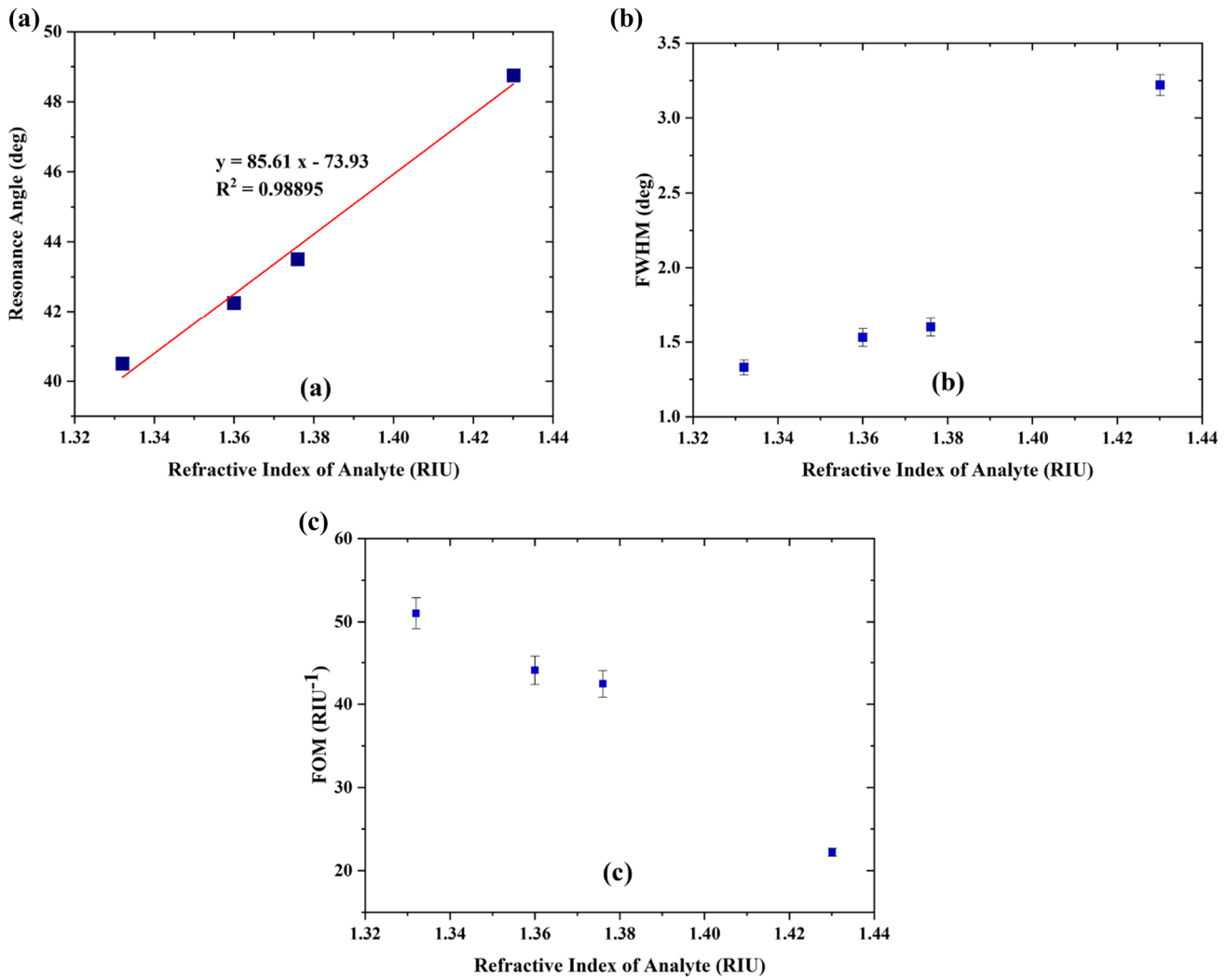

Fig. 12 Changes in the resonance angle and the corresponding linear fitting (**a**), FWHM (**b**), and FOM (**c**) with variations in the RI of the analyte of proposed sensor

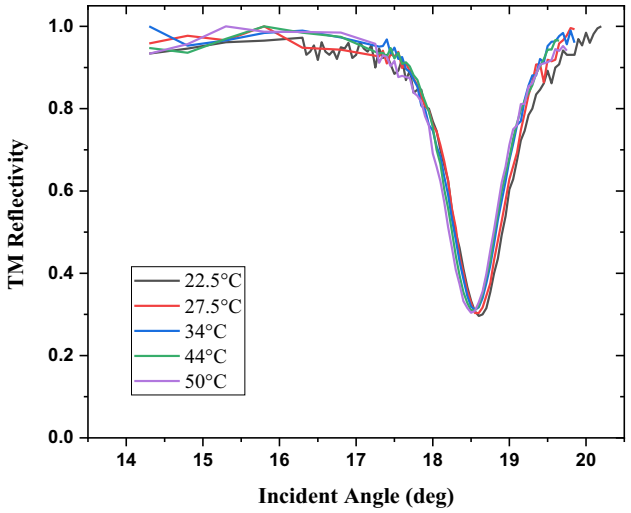

Fig. 13 Experimental SPR curves for different temperatures of plasmonic chip and instrument from 22.5 to 50 °C. The structure is an Ag-MgF_2 grating with a period, Λ, of 900 nm with 65 nm silver grating thickness and 15 nm MgF_2 thickness on a glass substrate

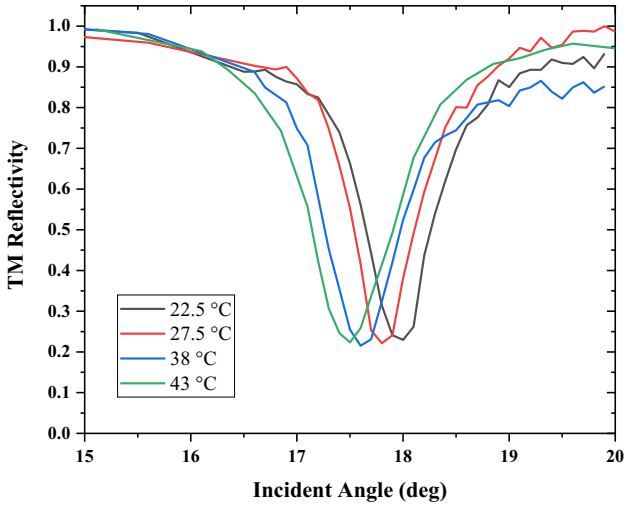

Fig. 14 Experimental SPR curves for different temperatures of the sensor set from 22.5 to 43 °C. The investigated structure is an Ag-MgF_2 grating with a period, Λ, of 900 nm with 65 nm silver grating thickness and 15 nm MgF_2 thickness on a glass substrate

of thermoelectric cooler, fan, and heat sink. At first, only the temperature of the plasmonic chip and instrument was changed and the SPR angular spectrum was recorded with steps of 0.1 degrees (Fig. 13). The structure investigated is an Ag-MgF_2 grating with a period, Λ, of 900 nm, 65 nm silver grating thickness, a 15 nm MgF_2 thickness, glass substrate, and an air analyte. This figure shows no significant change in the SPR response. With a temperature change of 22.5°–50 °C, the resonant angle will shift from 18.6° to 18.5°. In fact, the rate of resonant angle changes with temperature is − 0.0036 deg/°C and it confirms that the contribution of the instrument sensitivity to temperature is negligible for the SPR sensor with grating coupler.

In the next step, in addition to changing the temperature of the plasmonic chip and instrument, the temperature of the test chamber was also changed and the SPR response was recorded (Fig. 14). The figure shows that in this case, the change in the SPR response was higher than that of the previous one which indicates the effect of the temperature of the analyte on the resonance curve.

Figure 14 shows the variations of the resonance angle for different temperatures of the analyte chamber. We observe a left-handed shift with elevation of temperature. With a variation in temperature from 22.5° to 43 °C, the resonant angle will shift from 18 degrees to 17.5 degrees. The fitting line between the resonant angle and the temperature indicates that in this case, the resonant angle decreases with the rate of 0.02 deg/°C with the increase of temperature. This rate is 5 times more than that of the previous case which can be attributed to the change in the RI of analyte with temperature. It shows that when used as a gas alloy sensor, the sensor has lower temperature dependence than the fluid sensor. The reason for the shift in the resonance angle in Fig. 14 compared with Fig. 13 is the optical window. Also, the results show that in this temperature range, the resonant width will not change considerably.

4 Conclusion

A high sensitivity and high dynamic range surface plasmon resonance sensor based on one-dimensional metallic grating was designed and fabricated. Since the sensitivity of the sensor decreases due to oxidation, to prevent silver oxidation, suitable-thickness MgF_2 was coated on the silver grating while examining its plasmonic properties and finally an Ag-MgF_2 grating-based sensor was proposed. The angular modulation approach was used to evaluate the performance of the sensor**.** The sensitivity of the proposed sensor calculated by fitting line was 85.61 deg/RIU. Also, the figure of merit of the proposed sensor approached 51 RIU^{-1} that showed the proposed sensor had higher sensitivity and FOM in comparison to the experimental cases reported so far. It was shown that by optimization of the silver-based sensor, it has great potential for use in sensor applications. Given that a wide range of biomolecules have a refractive index of 1.3–1.6 RIU, this sensor can be very useful for their detection. With an increase in RI of analyte, the FWHM of the SPR curve increased and subsequently FOM decreased. Based on the made grating pattern, the sinusoidal profile was

considered for simulation with a relatively good conformity with the experimental results. The effect of temperature on the operation of the sensor was also investigated. The final results show that when the temperature rises, the resonant angle shifts to larger angles. From the results of the measurements, it can be seen that temperature changes in the analyte refractive index have the most effect on the variations of the SPR response with temperature. It was shown that the changes in the resonance angle with the temperature in this structure were equal to 0.0036 deg/°C and 0.02 deg/°C for the temperature changes of plasmonic chip and sensor set, respectively. Also, the results showed that in the temperature range studied, the resonant width did not change considerably.

Acknowledgements The work was supported by University of Isfahan, Department of Physics.

Compliance with ethical standards

Conflict of interest The authors declare no conflict of interest.

References

1. M. Citartan, S.C. Gopinath, J. Tominaga, T.-H. Tang, Label-free methods of reporting biomolecular interactions by optical biosensors. Analyst **138**(13), 3576–3592 (2013)
2. H. Farmani, A. Farmani, Z. Biglari, A label-free graphene-based nanosensor using surface plasmon resonance for biomaterials detection. Phys. E Low-dimens. Syst. Nanostruct. **116**, 113730 (2020)
3. T. Arakawa, H. Yasukawa, K. Fujimoto, Detection of alcohol vapor using surface plasmon resonance sensor with organic-inorganic hybrid layers. Sens. Mater. **22**(4), 201–209 (2010)
4. G. Dharmalingam, N.A. Joy, B. Grisafe, M.A. Carpenter, Plasmonics-based detection of H_2 and CO: discrimination between reducing gases facilitated by material control. Beilstein J. Nanotechnol. **3**(1), 712–721 (2012)
5. A. Abbas, M.J. Linman, Q. Cheng, New trends in instrumental design for surface plasmon resonance-based biosensors. Biosens. Bioelectron. **26**(5), 1815–1824 (2011)
6. P.K. Teotia, R. Kaler, 1-D grating based SPR biosensor for the detection of lung cancer biomarkers using Vroman effect. Opt. Commun. **406**, 188–191 (2018)
7. R. Wang, W. Wang, H. Ren, J. Chae, Detection of copper ions in drinking water using the competitive adsorption of proteins. Biosens. Bioelectron. **57**, 179–185 (2014)
8. B.J. Yakes, J. Deeds, K. White, S.L. DeGrasse, Evaluation of surface plasmon resonance biosensors for detection of tetrodotoxin in food matrices and comparison to analytical methods. J. Agric. Food Chem. **59**(3), 839–846 (2010)
9. Z. Altintas, Surface plasmon resonance based sensor for the detection of glycopeptide antibiotics in milk using rationally designed nanoMIPs. Sci. Rep. **8**(1), 11222 (2018)
10. Z. Samavati, A. Samavati, A. Ismail, M.A. Rahman, M.H.D. Othman, Detection of saline-based refractive index changes via bilayer ZnO/Ag-coated glass optical fiber sensor. Appl. Phys. B **125**(9), 161 (2019)
11. A. Farmani, A. Mir, Graphene sensor based on surface plasmon resonance for optical scanning. IEEE Photon. Technol. Lett. **31**(8), 643–646 (2019)
12. J. Zhu, L. Qin, S. Song, J. Zhong, S. Lin, Design of a surface plasmon resonance sensor based on grating connection. Photon. Sens. **5**(2), 159–165 (2015)
13. Z. Sadeghi, H. Shirkani, High-performance label-free near-infrared SPR sensor for wide range of gases and biomolecules based on graphene-gold grating. Plasmonics **14**(5), 1179–1188 (2019)
14. A. Takeda, T. Aihara, M. Fukuhara, Y. Ishii, M. Fukuda, Schottky-type surface plasmon detector with nano-slit grating using enhanced resonant optical transmission. J. Appl. Phys. **116**(8), 084313 (2014)
15. C. Ropers, C. Neacsu, T. Elsaesser, M. Albrecht, M. Raschke, C. Lienau, Grating-coupling of surface plasmons onto metallic tips: a nanoconfined light source. Nano Lett. **7**(9), 2784–2788 (2007)
16. H. Shen, B. Maes, Combined plasmonic gratings in organic solar cells. Opt. Express **19**(106), A1202–A1210 (2011)
17. J. Homola, S.S. Yee, G. Gauglitz, Surface plasmon resonance sensors. Sens. Actuators B Chem. **54**(1–2), 3–15 (1999)
18. X. Liang, A. Liu, C. Lim, T. Ayi, P. Yap, Determining refractive index of single living cell using an integrated microchip. Sens. Actuators A **133**(2), 349–354 (2007)
19. W.J. Choi, D.I. Jeon, S.-G. Ahn, J.-H. Yoon, S. Kim, B.H. Lee, Full-field optical coherence microscopy for identifying live cancer cells by quantitative measurement of refractive index distribution. Opt. Express **18**(22), 23285–23295 (2010)
20. C. Lenaerts, F. Michel, B. Tilkens, Y. Lion, Y. Renotte, High transmission efficiency for surface plasmon resonance by use of a dielectric grating. Appl. Opt. **44**(28), 6017–6022 (2005)
21. K.H. Yoon, M.L. Shuler, S.J. Kim, Design optimization of nano-grating surface plasmon resonance sensors. Opt. Express **14**(11), 4842–4849 (2006)
22. K. Lin, Y. Lu, J. Chen, R. Zheng, P. Wang, H. Ming, Surface plasmon resonance hydrogen sensor based on metallic grating with high sensitivity. Opt. Express **16**(23), 18599–18604 (2008)
23. T. Kan, N. Tsujiuchi, E. Iwase, K. Matsumoto, I. Shimoyama, Planar near-infrared surface plasmon resonance sensor with Si prism and grating coupler. Sens. Actuators B Chem. **144**(1), 295–300 (2010)
24. A. Dhawan, M. Canva, T. Vo-Dinh, Narrow groove plasmonic nano-gratings for surface plasmon resonance sensing. Opt. Express **19**(2), 787–813 (2011)
25. A. Arriola, A. Rodriguez, N. Perez, T. Tavera, M.J. Withford, A. Fuerbach et al., Fabrication of high quality sub-micron Au gratings over large areas with pulsed laser interference lithography for SPR sensors. Opt. Mater. Express **2**(11), 1571–1579 (2012)
26. F. Wu, L. Liu, L. Feng, D. Xu, N. Lu, Improving the sensing performance of double gold gratings by oblique incident light. Nanoscale **7**(30), 13026–13032 (2015)
27. A. Bijalwan, V. Rastogi, Sensitivity enhancement of a conventional gold grating assisted surface plasmon resonance sensor by using a bimetallic configuration. Appl. Opt. **56**(35), 9606–9612 (2017)
28. M.S. Hamed, G.T. Mola, Copper sulphide as a mechanism to improve energy harvesting in thin film solar cells. J. Alloy. Compd. **802**, 252–258 (2019)
29. S.O. Oseni, G.T. Mola, Bimetallic nanocomposites and the performance of inverted organic solar cell. Compos. B Eng. **172**, 660–665 (2019)
30. M.W. Dlamini, G.T. Mola, Near-field enhanced performance of organic photovoltaic cells. Phys. B **552**, 78–83 (2019)
31. S.Y. Lee, J.J. Amsden, S.V. Boriskina, A. Gopinath, A. Mitropolous, D.L. Kaplan et al., Spatial and spectral detection of protein monolayers with deterministic aperiodic arrays of metal

nanoparticles. Proc. Natl. Acad. Sci. **107**(27), 12086–12090 (2010)
32. P.B. Johnson, R.-W. Christy, Optical constants of the noble metals. Phys. Rev. B **6**(12), 4370 (1972)
33. W. Luo, R. Wang, H. Li, J. Kou, X. Zeng, H. Huang et al., Simultaneous measurement of refractive index and temperature for prism-based surface plasmon resonance sensors. Opt. Express **27**(2), 576–589 (2019)
34. M. Zekriti, Temperature effects on the resolution of surface-plasmon-resonance-based sensor. Plasmonics **14**(3), 763–768 (2019)